Origin of the uniaxial magnetic anisotropy in $La_{0.7}Sr_{0.3}MnO_3$ on stripe-domain $BiFeO_3$

Lu You,[1] Baomin Wang,[1,2] Xi Zou,[1] Zhi Shiuh Lim,[1] Yang Zhou,[1] Hui Ding,[1] Lang Chen,[1,3] and Junling Wang[1,*]

[1]*School of Materials Science and Engineering, Nanyang Technological University, Singapore 639798, Singapore*

[2]*Ningbo Institute of Materials Technology & Engineering, Chinese Academy of Sciences, Ningbo 315201, P.R. China*

[3]*South University of Science and Technology of China, Shenzhen 518055, P.R. China*

(Received 19 September 2013; published 25 November 2013)

The $La_{0.7}Sr_{0.3}MnO_3/BiFeO_3$ (LSMO/BFO) heterostructure has been a model system to study the interaction between ferroic order parameters at a complex oxide interface. In this study, uniaxial magnetic anisotropy is artificially induced in LSMO thin film grown on BFO with electrically patterned stripe domains. Variable-field magnetic force microscopy is exploited to investigate the *in situ* magnetic switching dynamics and subsequently determine the magnetic easy axis of the LSMO thin film. Intriguingly, one-to-one correspondence between the magnetization of LSMO and the polarization of BFO is found. The observed uniaxial magnetic anisotropy is attributed to the magnetocrystalline anisotropy of the LSMO, which is induced by the shear strain of the BFO lattice, rather than the interfacial magnetic coupling which would be more naturally assumed. This finding highlights the crucial role of lattice coupling at a complex oxide interface. When multiple-order parameters come into play at the heterointerface, special care is needed to deconvolute their effects on the related physical properties.

DOI: 10.1103/PhysRevB.88.184426 PACS number(s): 75.30.Gw, 77.80.bn, 77.80.Dj, 75.70.−i

I. INTRODUCTION

Heteroepitaxial oxide interfaces have gradually become the frontier in condensed-matter science for exploring emergent phenomena with new physics and functionalities in recent years.[1–4] This is facilitated by great advances in thin film growth techniques that enable the fabrication of artificial heterointerfaces with atomic-scale precision.[5–7] Due to the intrinsic symmetry breaking at the interface, unique properties that are absent in bulk materials can be created at the heteroepitaxial boundaries through the interplay between charge, spin, orbital, and lattice degrees of freedom. The heterointerface between multiferroic $BiFeO_3$ (BFO) and ferromagnetic $La_{0.7}Sr_{0.3}MnO_3$ (LSMO), a model system for studying cross-coupling between different ferroic order parameters, is attracting much attention because of its great potential for electrical control of magnetism in voltage-controlled magnetic devices with low power consumption.[8] It is reported that the observed large exchange bias in the LSMO/BFO heterostructure originates from the orbital reconstruction of the $3d$ Fe^{3+} and Mn^{3+}/Mn^{4+} ions at the interface.[9] More intriguingly, the exchange bias can be further modulated by electrical switching of the polarization of BFO, making an essential step toward magnetoelectric memory devices.[10,11] However, the exchange bias only exists in ultrathin LSMO films (2–10 nm) and at low temperature (blocking temperature $T_B \sim 100$–120 K), suggesting a strong decay of the exchange coupling against elevated temperature.[9,10,12] Instead of unidirectional anisotropy, we have previously shown that room temperature uniaxial magnetic anisotropy can be introduced in a relatively thick LSMO layer (∼30 nm) grown on a BFO layer with regular ferroelectric stripe domains.[13] Thus, it is intuitively expected that the induced magnetic anisotropy is due to the magnetic exchange coupling at the LSMO/BFO interface. However, since the ferroelastic, ferroelectric, and antiferromagnetic orders in BFO are intimately linked, the effect of ferroelasticity/strain on the magnetic property of LSMO cannot be excluded. Moreover, due to the large differences in the thickness and temperature scales between our study and those reported in literature, the observed unidirectional or uniaxial anisotropies in LSMO/BFO heterostructures may have completely different origins. In our LSMO/BFO bilayer, although the anisotropy due to the vicinal substrate has been carefully ruled out,[13] it is still unclear whether the underpinning mechanism is an elastic or magnetic coupling in nature. Besides, a microscopic picture of the coupling between the local polarization of BFO and the magnetic moment of LSMO remains elusive.

To shed some light on these problems, we have induced local magnetic anisotropy in LSMO thin film by depositing it on top of BFO with electrically poled stripe domains. Using variable-field magnetic force microscopy (VF-MFM),[14–16] the evolution of the magnetic domain structures of the LSMO thin film during magnetization switching was examined, with the magnetic easy axis determined. Interestingly, the ferromagnetic domains in LSMO and the ferroelectric domains in BFO are correlated one-to-one. By excluding the interfacial magnetic coupling as the origin, the observed uniaxial magnetic anisotropy is ascribed to the magnetocrystalline anisotropy due to the lattice coupling across the LSMO/BFO heterointerface. Our finding provides new insights into LSMO/BFO, as well as other complex oxide heterostructures, where multiple-order parameters coexist. To achieve better understanding of the physical properties, it is crucial to deconvolute their effects at different temperature and dimension scales.

II. EXPERIMENTAL METHODS

BFO thin film 40–50 nm thick was first deposited onto nominal exact (001)-oriented $SrTiO_3$ (STO) substrate by pulsed laser deposition at 700 °C and under an oxygen partial pressure of 100 mTorr. Subsequently, parallel Pt electrodes with channel widths around 4–6 μm were patterned on top using photolithography. An external electric field was applied between the electrode pair to switch ferroelectric domains of the BFO film into a highly aligned stripe pattern. Finally,

30-nm-thick LSMO thin film was grown on top at 650 °C and under an oxygen partial pressure of 300 mTorr.

The topographic imaging, piezoelectric force microscopy (PFM), and VF-MFM were all carried out on a commercial atomic force microscope (MFP3D, Asylum Research). During PFM scan, the Pt-coated probe (DPE 14, Mikromasch) was driven at an ac voltage of 2 V and a frequency of 10 kHz. In VF-MFM, the magnetic field was controlled by two motorized permanent magnets, and calibrated by a gaussmeter. A high-coercivity (>5000 Oe) magnetic probe with CoPt/FePt coating (ASYMFMHC, Asylum) was used to prevent a disturbance from the external magnetic field and stray field of the sample. The MFM is carried out under a dual-pass scan with a lift height of 30–50 nm. The image contrast is calculated by the standard deviation of the MFM phase signal. Macroscopic magnetic hysteresis loops were measured by a vibrating sample magnetometer (LakeShore 7400) at room temperature. After all the experiments, the LSMO layer was chemically removed using 10 weight percent (wt%) KI + 10 wt% HCl solution to expose the BFO surface for PFM rescan.

III. RESULTS AND DISCUSSION

A. LSMO growth on an electrically poled BFO surface

In order to exclude any possible anisotropy resulting from the substrate, nominal *exact* (001)-oriented STO was used for sample preparation. As schematically shown in Fig. 1(a), 40–50-nm-thick BFO film was first deposited on nominal exact STO substrate. The in-plane PFM image [Fig. 1(b)] shows a typical domain structure with all four structural variants.[17–19] The out-of-plane polarization component (not shown) is pointing upward and remains unchanged throughout the whole experiment. As reported in our previous study, such an isotropic domain pattern of BFO film cannot introduce uniaxial magnetic anisotropy in LSMO grown on top.[13] To induce domain anisotropy, Pt electrodes (with a channel length of 100 μm and a gap of 4–6 μm) were lithographically patterned on top of BFO subsequently. Upon applying an in-plane electric field between the Pt electrodes, the BFO film within the channel can be switched into highly aligned stripe domains, while the domain structures outside the channel area remain unaffected. As shown in Fig. 1(d), the stripe domains consist of two structural variants with a zigzag-like head-to-tail connection of the polarization vectors, leading to a net polarization direction along the applied electric field.[19] Finally, a 30-nm-thick LSMO film was grown on the whole surface of BFO, including the major unpoled area (isotropic domain pattern) and the prepoled channel area (anisotropic stripe domain). As shown in Figs. 1(c) and 1(e), the film topography within the prepoled channel area is largely preserved after LSMO growth, with no detectable anisotropy. However, stripe-like features similar to the ferroelectric domains of BFO can be observed in the corresponding MFM image within the channel area, although with less order. It should be noted that the growth temperature for LSMO (~650 °C) is well below the ferroelectric Curie temperature of BFO (>800 °C).[20] Therefore, the electrically switched ferroelectric stripe domains can be maintained during and after LSMO growth. This is further confirmed by subsequent experiments as described below. A similar result was obtained if the BFO was poled in the opposite direction (see Supplemental Material, Fig. S1[21]). On the other hand, the MFM image of an unpoled channel area exhibit mosaic magnetic domains with no preferred orientation (see Supplemental Material, Fig. S2[21]). This raises one question: Does the LSMO layer exhibit similar striped magnetic domains that correlate with

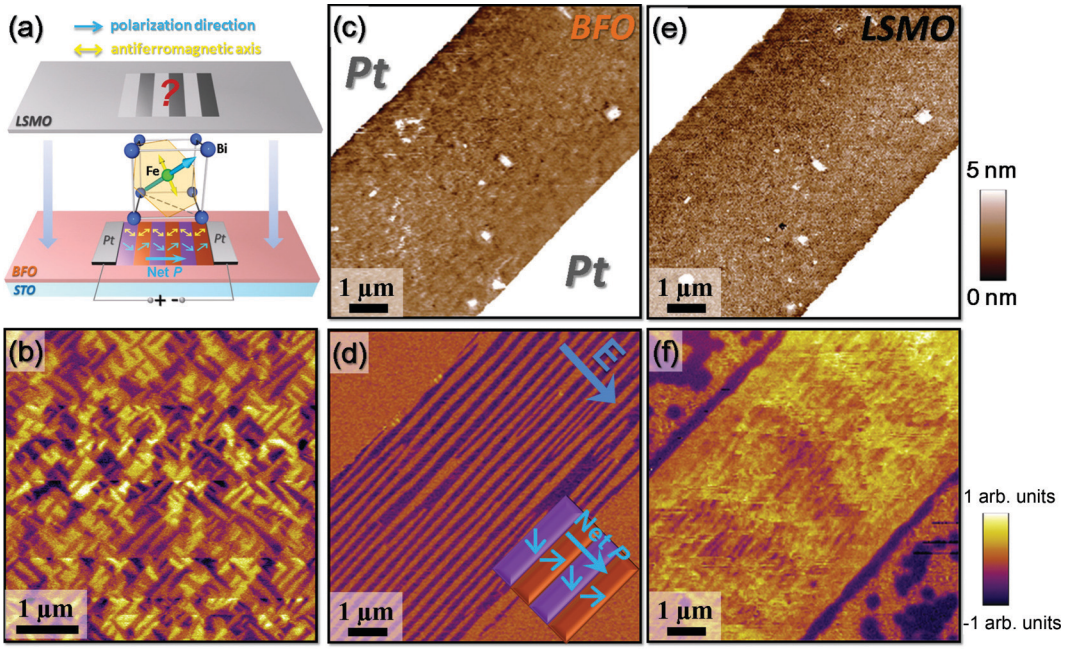

FIG. 1. (Color online) (a) Schematic diagram of the sample structure. The BFO unit cell shows the cross-coupling between polarization and antiferromagnetism. (b) In-plane PFM image of the as-grown BFO film. (c) Topographic and (d) in-plane PFM images of the BFO film after electrical switching. (e) Topographic and (f) corresponding MFM images of the LSMO film grown on top of the poled BFO.

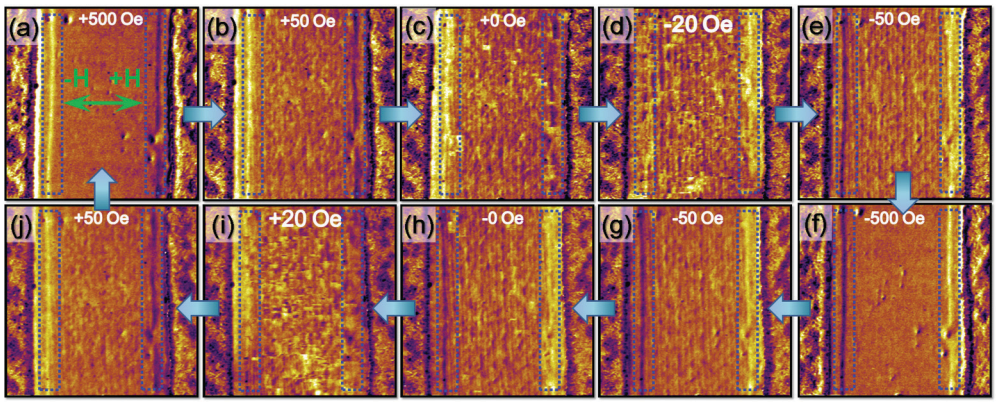

FIG. 2. (Color online) (a–j) Domain evolution of the LSMO layer when the magnetic field is sweeping parallel to the net polarization direction. All the MFM images are 8 μm $\times$ 8 μm, and with the same phase scale (0.5°). The blue dotted boxes denote two lines with uncompensated stray fields located at two ends of the channel.

the ferroelectric domains of the underlying BFO layer in the prepoled area?

B. Study of magnetic domain dynamics using VF-MFM

To reveal more information on the magnetic domain structures of the LSMO layer, magnetization switching dynamics were investigated using VF-MFM with the magnetic field H parallel or perpendicular to the direction of net polarization (P_{net}). The corresponding domain evolutions are demonstrated in Figs. 2 and 3 with the field-sweeping sequence indicated by the arrows (see the movies in Supplemental Material[21]). In MFM images, the contrast results from the out-of-plane magnetostatic interaction between the sample and the magnetized probe.[22] Typically, LSMO thin film under tensile strain (a_{LSMO} = 3.873 Å, a_{STO} = 3.905 Å) exhibits strong in-plane magnetic anisotropy. Thus, only the stray fields emanating from the magnetic domain boundaries can be detected by the magnetized probe.[15] Specifically in our MFM images (phase signal), yellow (bright) and purple (dark) tones indicate attractive (south pole) and repulsive forces (north pole), respectively.

In the parallel field case (Fig. 2), almost no contrast can be observed in the MFM image at high positive field (+500 Oe), except those due to the surface particles. Besides, two lines with opposite contrast (indicated by blue dashed boxes) can be clearly seen at both sides of the channel. This could be due to the uncompensated stray fields at the two boundaries of the channel. As the field decreases, the contrast of the MFM image gradually increases, with a more and more noticeable stripelike feature. Upon reversing the field, magnetization switching occurs around -20 Oe, which can be inferred from the contrast switching of the two lines at both sides. A further increase of the negative field leads to reduced contrast again. When sweeping the field from negative maximum to positive maximum, the domain evolution shows similar behavior, with the switching occurring at around $+20$ Oe. If the contrast of the MFM image (defined as the standard deviation of the phase signal) is plotted against the sweeping magnetic field, as shown in Fig. 4(a), the derived hysteretic curve exhibits two distinct peaks at around ± 20 Oe, which corresponds to the coercive field of the film within the channel. The shape of the curve is reminiscent of the typical susceptibility hysteresis loop of a ferromagnetic material, namely the first derivative of the magnetization hysteresis loop. This can be understood in terms of the imaging mechanism of MFM. First, the magnetized probe mainly senses the stray fields from the domain walls. During the magnetization switching process, more domain

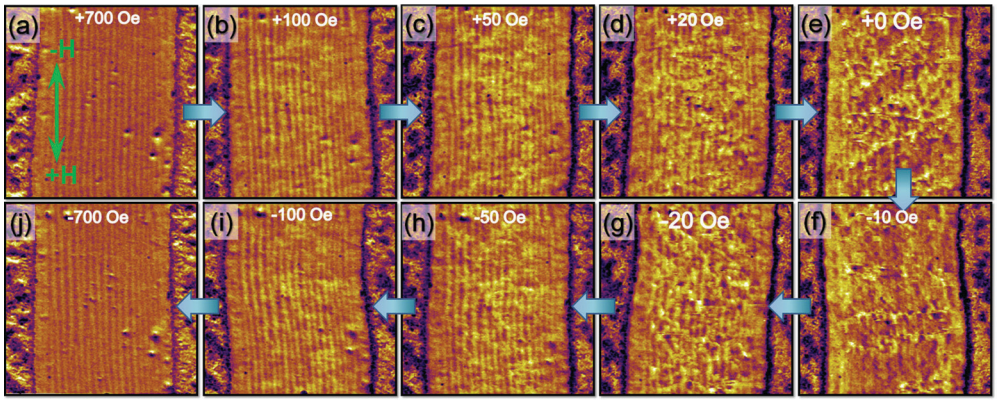

FIG. 3. (Color online) (a–j) Domain evolution of the LSMO layer when the magnetic field is sweeping perpendicular to the net polarization direction. All the MFM images are 8 μm $\times$ 8 μm, and with the same phase scale (0.5°).

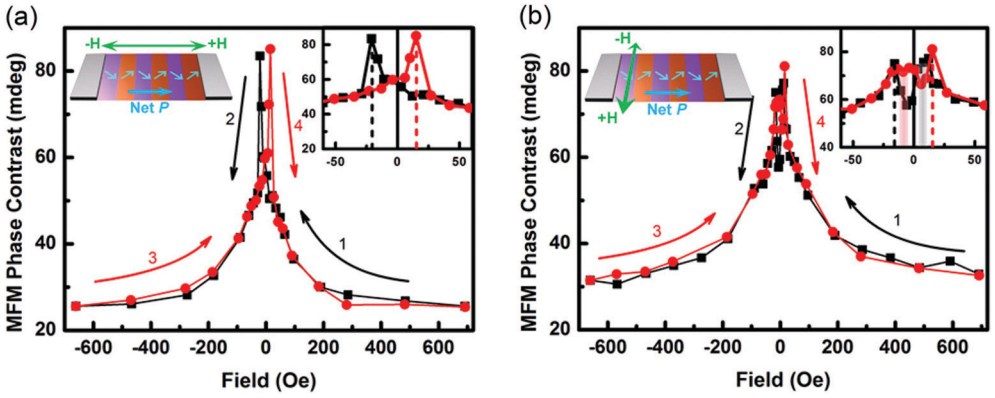

FIG. 4. (Color online) Contrast variations of the MFM images as a function of the sweeping magnetic field for (a) parallel and (b) perpendicular conditions. The insets are the zoomed-in images of the low-field regions.

boundaries will form, giving rise to greatly enhanced contrast in MFM images. Conversely, under high magnetic field, all the magnetic moments align with the external field to reduce the Zeeman energy, thus leading to the vanishing of stray fields and image contrast. Furthermore, the moving probe is considered as a tiny bar magnet that produces a localized field that interacts with the sample. Increasing susceptibility close to the coercive field will also result in enhanced probe-sample interaction and image contrast accordingly.[23]

If the magnetic field is applied along the perpendicular direction, similar behavior is observed: The MFM image contrast minimizes at high field, whereas it increases when switching takes place (Fig. 3). However, even with a field as high as 700 Oe, magnetic stripe domains mimicking the ferroelectric domains of BFO are still visible, implying that the magnetization is still not completely aligned with the external field. Moreover, after quantifying the image contrast with regard to the magnetic field, four peaks instead of two are identified at low field [inset of Fig. 4(b)]. In addition to the two peaks that correspond to the coercive field, two broadened peaks close to zero field appear first when the field is sweeping from positive (negative) maximum to negative (positive) maximum. As for the major unpoled area outside the channel, the BFO film exhibits no anisotropy in the ferroelectric domain pattern, as shown in Fig. 5(a). This is consistent with the macroscopic magnetization measurements: The majority of the LSMO film exhibits identical M-H loops along the two in-plane axes [Fig. 5(c)]. We also collected the contrast evolution for the unpoled area using VF-MFM. By comparing with the data of the prepoled area, it is shown that the image contrasts have distinct values in the high-field region for these three situations [Fig. 5(d)]. For LSMO film within the channel, the high-field contrast is largest when a field is applied perpendicular to P_{net}, indicating that magnetization aligned in this direction is the most difficult. Conversely, the high-field contrast is minimum and well-saturated in the parallel direction, suggesting an easy magnetic axis along this direction. Accordingly, the easy and hard axes of LSMO film within the channel can be determined. This induced magnetic anisotropy is in complete agreement with our previous result.[13] It further confirms that the magnetic anisotropy of LSMO grown on stripe-domain BFO has nothing to do with the substrate miscut but is closely related to the domain structure of BFO film. The only difference is that, in our previous work, the stripe domains of BFO are created by the substrate vicinality, whereas in this paper, the stripe domains are created by an external electric field. For the film outside the channel, no uniaxial anisotropy exists. As a result, the image contrast has an intermediate value.

C. Resolving magnetic easy axes in LSMO

Next, we investigate the detailed magnetic domain structures of the LSMO film by looking into the zoomed-in MFM images. As described above, when the external field is applied along the perpendicular direction, magnetic stripe domain patterns persist even at high magnetic field. Reversing the field leads to almost identical stripe domain pattern [Figs. 6(a) and 6(c)]. However, if we compared the line profiles of the MFM images at the same spatial position under positive and negative fields, it can be found that they show completely opposite MFM signals [Fig. 6(b)]. This is done by taking advantage of the topographic features as the reference points, as indicated by the blue circles in Figs. 6(a) and 6(c). The switching of the MFM phase signal indicates that the polarity of the stray field at the magnetic domain wall reverses with the magnetic field. To explain this observation, first recall the microscopic model proposed in Ref. 13, where the LSMO layer grown on top of striped-domain BFO also forms magnetic stripe domains with zigzag magnetic easy axes, as delineated by the red dotted arrows in Fig. 6(e). At high field, the magnetic moments tend to align to the field direction. However, they cannot be aligned completely parallel to the field due to the large anisotropy energy. This results in head-to-head/tail-to-tail charged domain walls with out-of-plane stray fields that manifest themselves as periodically alternating contrasts in the MFM images. Once the external field is reversed, the magnetic moments will also flip, causing reversal of the magnetic polarity at the domain wall. On the other hand, when the applied field is along the parallel direction, as shown in Fig. 6(d), the MFM image shows a stripe domain pattern with less order, and more stripes seem to appear. This can be understood based on the formation of 90° Néel walls between adjacent ferromagnetic domains, which are more energetically

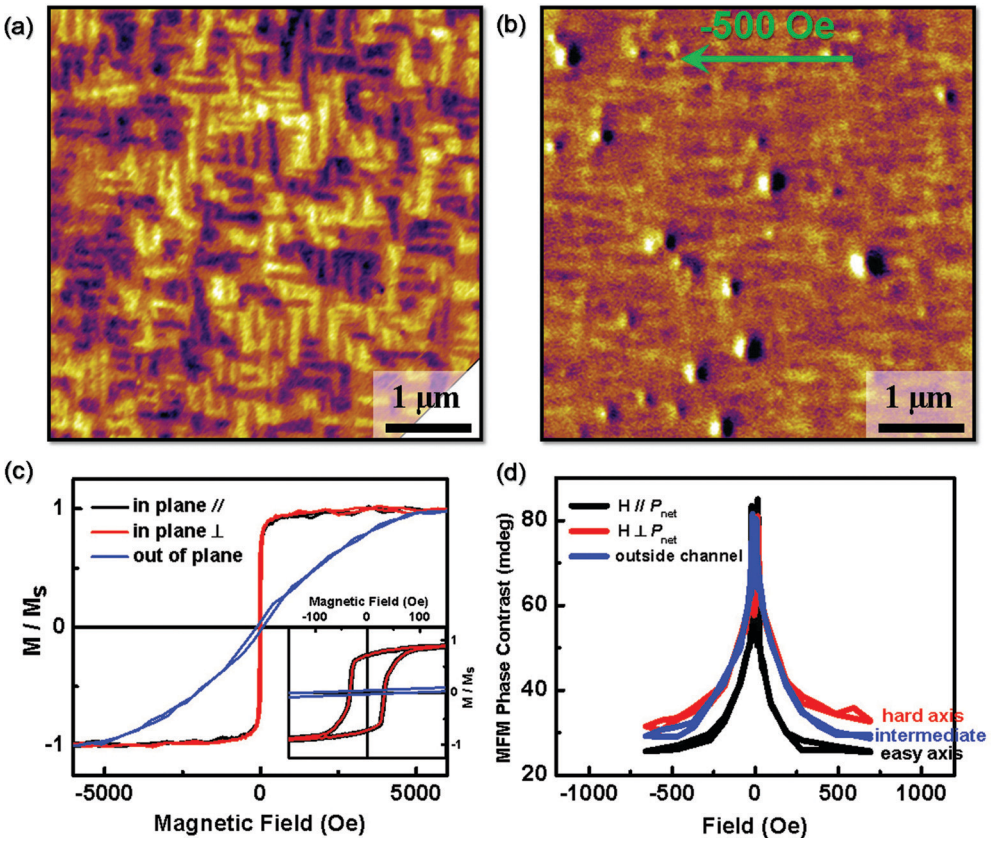

FIG. 5. (Color online) (a) PFM image of the unpoled region of BFO thin film and (b) corresponding MFM image of LSMO grown on top under a high magnetic field. (c) Macroscopic magnetic hysteresis loops of the entire sample along out-of-plane and two orthogonal in-plane directions. The inset shows the zoomed-in part. (d) Comparison of the MFM image contrasts for three different cases.

favorable in thin ferromagnetic films. As illustrated in Fig. 6(f), the stray field of each 90° Néel wall will produce a maximum and a minimum in the MFM image contrast.[24,25] Therefore, the stripe number in the image appears to be doubled. The disorder of the stripe pattern in this case could be due to the poorer sensitivity to the 90° Néel walls in MFM and possibly finer magnetic structures.[26]

Based upon the derived magnetic structures of the LSMO layer, the scenario of the magnetic switching process can be reproduced in accordance with the VF-MFM images. It is relatively straightforward for the parallel field case, as schematically shown in Fig. 7(a). At large positive field, magnetic moments align nearly in a head-to-tail fashion, with almost zero contrast in the MFM image. When the field goes down to zero, the moment in each single domain gradually rotates back to its magnetic easy axis due to the anisotropy energy and forms 90° Néel walls with each other at the remanent state. The magnetic switching takes place sharply at around -20 Oe, where highest contrast is observed in the MFM image. The magnetic moments are fully reversed when passing the coercive field, and gradually align with the increasing magnetic field. In contrast, the switching behavior along the perpendicular direction is more complicated, as illustrated in Fig. 7(b). At large positive field, the magnetic moments deviate from their easy axes so as to maximally align with the external field, leading to the observed striped domain walls. The magnetic moments gradually rotate back to the easy axis with decreasing magnetic field due to the anisotropy energy. Once the field strength (around $+10$ Oe) is not enough to maintain the energetically unfavorable head-to-head/tail-to-tail arrangement, magnetization flips occur, which gives rise to the first peak shown in Fig. 4(b). The magnetic moments rearrange to form low-energy head-to-tail configurations at the remanence with reducing out-of-plane stray fields. That is why a decrease in the MFM image contrast is observed at zero field. At negative coercive field, a second magnetic switching is triggered, as evidenced by the second peak in the MFM contrast. Subsequently, the magnetic moments align with increasing external field through a similar rotation process. The domain evolutions under VF-MFM are thus self-consistently elucidated based on the model proposed.

D. Correlations between magnetic and ferroelectric stripe domains

Aiming to unravel the relationship between the magnetic domains of LSMO and the ferroelectric domains of BFO, we revisited the underlying BFO by selectively etching away the LSMO layer using a chemical method (see Experimental Methods). As shown in Fig. 8(b), the ferroelectric stripe domains indeed remain intact after high-temperature growth of the LSMO layer, indicating the robust stability of BFO ferroelectric domains against thermal fluctuation. Interestingly, when compared to the corresponding MFM image under a

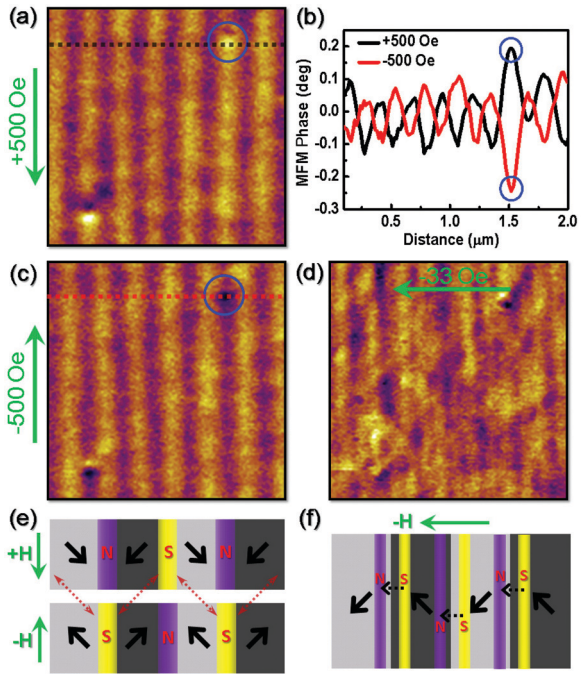

FIG. 6. (Color online) Zoomed-in MFM images of the LSMO layer under (a) positive and (b) negative magnetic field along the perpendicular direction. (c) Corresponding line profiles as shown in panels (a) and (b). The blue circles indicate the marking position for comparison. (d) Zoomed-in MFM images of the LSMO layer under parallel magnetic field. (e, f) Schematic diagrams showing the mechanisms of the contrast formation in the MFM images under perpendicular and parallel fields. The scan size for all MFM images is 2 μm × 2 μm.

perpendicular magnetic field, they match perfectly well with each other [Figs. 8(a) and 8(b)]. In fact, such good correlation can also be seen in the unpoled BFO region [Figs. 5(a) and 5(b)], but only for those stripe domains parallel to the magnetic

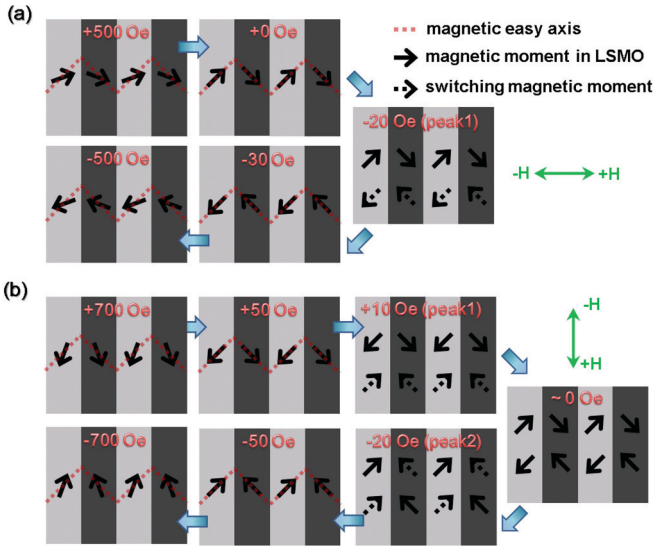

FIG. 7. (Color online) Step-by-step schematics showing magnetic moment arrangements in the uniaxial anisotropic LSMO film during the magnetic switching process under (a) parallel and (b) perpendicular magnetic fields.

field. In the zoomed-in images, an equal number of stripes can be observed [Figs. 8(c) and 8(d)]. However, the stripes in the MFM image shift by half of the domain width when aligned to the PFM image [the same topographic features are denoted by the blue circles and the domain wall by the white dotted lines in Figs. 8(c) and 8(d)], because the largest magnetic signal comes from the domain wall rather than the center of the domain. Figure 8(e) presents a three-dimensional view of the one-to-one correspondence between the magnetic and ferroelectric domains overlaid on the film topographies. Consequently, the orientation relationship between the magnetic easy axis in LSMO and the polarization vector in BFO can be determined. As depicted by the arrows in Figs. 8(c), 8(d), and 8(e), they are in fact parallel to each other. This conclusion is further confirmed in the sample with net polarization opposite of BFO (see Supplemental Material, Fig. S3[21]). Finally, in order to examine whether the magnetic anisotropy stems from magnetic exchange coupling at the interface, a thin nonmagnetic STO layer is inserted between the BFO and LSMO layers. As the strength of the exchange coupling decays exponentially with the increase of the thickness of the nonmagnetic spacer,[27] possible magnetic coupling between LSMO and BFO should be readily eliminated.[10,28] As shown in Fig. 8(f), the magnetic stripe domains in LSMO persist even after the insertion of the STO interlayer. Moreover, the magnetic easy axis of the LSMO and the polarization of BFO remain parallel. Similar results are obtained even when the thickness of the STO layer is increased from 2 to 5 nm. This finding unambiguously excludes the interface magnetic coupling as the origin of the uniaxial magnetic anisotropy in the LSMO film.

The results described above corroborate our previous study of macroscopic magnetization measurements from a microscopic point of view: The magnetic domain structure of LSMO completely follows the ferroelectric domain structure of BFO, and the zig-zag arrangement of the magnetic easy axes leads to an overall uniaxial magnetic anisotropy along the net polarization direction. A similar pattern transfer between a ferromagnet thin layer and a ferroelectric or multiferroic material has recently been reported in CoFe/$BiFeO_3$[29] and CoFe/$BaTiO_3$[30,31] systems. While in the former case, the uniaxial magnetic anisotropy is attributed to interface magnetic coupling, the latter case is claimed to originate from the ferroelastic strain of $BaTiO_3$.

Next, we shall discuss the origin of the magnetic anisotropy in our sample. Magnetic anisotropy of manganite thin films has been widely reported in the literature, including magnetocrystalline anisotropy modulated by epitaxial strain,[32,33] surface-step-induced anisotropy (shape anisotropy or strain-relaxation anisotropy),[34,35] and exchange anisotropy.[36,37] As mentioned above, low-temperature exchange bias was reported in LSMO/BFO heterostructures due to the interfacial hybridization between Mn and Fe $d_{3z^2-r^2}$ orbitals mediated by the oxygen $2p$ orbital.[9] Futhermore, such kinds of exchange coupling indeed show certain anisotropic characteristics along different crystallographic directions, which might be closely related to the domain structures of BFO.[11] However, if we try to evaluate the exchange energy of our LSMO/BFO sample at room temperature based on the well-known expression[38]

$$H_E = \frac{J_{INT}}{M_{FM} t_{FM}},$$

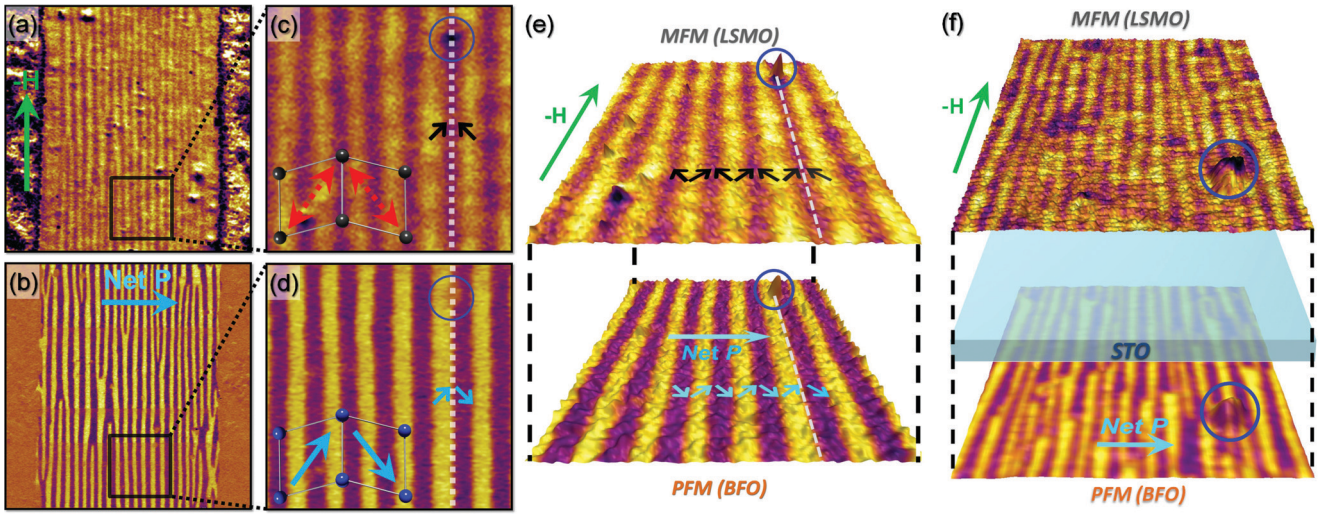

FIG. 8. (Color online) (a) MFM image of the LSMO layer under a perpendicular magnetic field and (b) PFM image of the underlying BFO layer exhibit identical stripe patterns. (c) Zoomed-in MFM image and (d) zoomed-in PFM image reveal the relationship between local polarization of BFO and the magnetic easy axis of LSMO. The distorted in-plane lattices of BFO and LSMO are also shown with the corresponding polarization vector and magnetic easy axis labeled by blue and red arrows, respectively. The blue circles and the dotted lines are guides to the eyes. (e) MFM and PFM signals in (c) and (d) overlaid on the corresponding topographic images of LSMO and BFO thin films to show the correlation. (f) Perspective view of three-dimensional topographic images of BFO and LSMO layers overlaid with corresponding PFM and MFM signals after inserting a thin nonmagnetic STO interlayer. The scan sizes are 8 μm × 8 μm in (a) and (b); 2 μm × 2 μm in (c), (d), and (e); and 4 μm × 4 μm in (f).

where J_{INT} is the interface coupling constant, M_{FM} is the saturation magnetization, and t_{FM} is the thickness of the ferromagnetic layer, we can see that the magnitude of the exchange field is inversely proportional to the thickness of the ferromagnetic layer and decays fast with elevated temperature due to the decrease in interface coupling strength. Considering the Curie temperature of LSMO (∼350 K) is close to the room temperature, the interface coupling is greatly reduced under the experimental condition. Furthermore, the relatively large thickness of our LSMO film also weakens the effect of interface coupling. This conclusion is further supported by the experimental results reported in the literature. For example, the exchange bias of LSMO on BFO can only be observed below ∼100 K with a thickness of LSMO below 10 nm,[9–12] and the coercive field of LSMO on BFO decays rapidly with increasing temperature.[9,12,13] All these observations support greatly weakened magnetic exchange coupling between BFO and LSMO at room temperature.

The magnetic coupling between BFO and LSMO is further ruled out by the fact that magnetic anisotropy persists even after the insertion of a nonmagnetic STO layer. It is reported that the strength of the exchange coupling decays exponentially with an increase in the thickness of the nonmagnetic spacer.[27] Thus, the insertion of a nonmagnetic STO interlayer is very efficient in killing the interface magnetic coupling, which has also been proved in BFO-based ferromagnetic/antiferromagnetic systems.[10,12,28] As a result, we can exclude magnetic coupling as the origin of the uniaxial magnetic anisotropy.

On the other hand, the uniaxial magnetic anisotropy of LSMO thin films induced by anisotropic elastic strain has been studied systematically on low-symmetry substrates.[33,39] It is found that the in-plane magnetic easy axis always lies along the direction of smallest compressive strain or largest tensile strain. The microscopic magnetocrystalline anisotropy is a result of the combined effects of crystal-field interaction and spin-orbit coupling. The anisotropic strain first causes the deformation of the MnO_6 octahedra, leading to alignment of the Mn orbitals in the LSMO crystal field. Subsequently, the spin-orbit coupling of these orbitals results in a magnetic easy axis with minimum energy. For fully strained BFO film grown on STO substrate, the in-plane lattice exhibits shear strain instead of biaxial strain due to the rhombohedrally distorted nature of the bulk unit cell.[18] As shown in Fig. 8(d), the in-plane polarization lies along the longer diagonal. Since both bulk BFO and LSMO adopt R-3c symmetry with $a^-a^-a^-$-type O_6 octahedral tilt,[40–42] the in-plane distortion of the LSMO unit cell should follow that of BFO due to the continuity of the lattice through the interface, as depicted in Fig. 8(c). As a consequence of the anisotropic tensile strain along the two in-plane diagonals, the magnetic easy axis of LSMO is expected to lie along the direction with larger tensile strain, namely, the longer diagonal. And this is in good agreement with our experimental result [Fig. 8(c)]. The ferroelectric stripe domains in BFO further lead to similar twinning domains in LSMO through one-to-one correlation of the lattice distortion. Thus, the magnetic easy axes of the LSMO domains also follow a zigzag arrangement, resulting in an overall magnetic easy axis parallel to the net polarization direction of BFO. Inserting a thin STO layer between LSMO and BFO should readily quench the magnetic exchange coupling at the heterointerface,[27] but not for the lattice strain. Therefore, we are able to conclude that the origin of the uniaxial magnetic anisotropy is elastic rather than magnetic in nature. Further detailed structural analyses are needed to corroborate this conclusion.

IV. CONCLUSION

LSMO thin film with local magnetic anisotropy has been artificially created on top of electrically poled BFO film. The anisotropic magnetic switching behavior of the LSMO layer was studied in detail using VF-MFM along two in-plane orthogonal directions. By carefully analyzing the MFM images, the magnetic easy axis can be identified in each magnetic domain. Accordingly, the domain evolution during magnetic switching is explained in line with the local domain configuration proposed. Furthermore, one-to-one correspondence between the magnetic stripe domains in LSMO and ferroelectric stripe domains in BFO can be found, with the magnetic easy axis parallel to the polarization direction. Last but not least, the origin of the magnetic anisotropy was discussed. Magnetic exchange anisotropy has been carefully ruled out by the insertion of a nonmagnetic STO interlayer, and the observed uniaxial magnetic anisotropy of LSMO is attributed to magnetocrystalline anisotropy due to the anisotropic tensile strain induced by the underlying BFO layer. These findings underscore the importance of lattice coupling at complex oxide heterointerfaces. When multiple-order parameters come into play at the heterointerface, disentangling their influences on the related physical properties at different temperature and dimension scales will be a crucial step toward better control of device applications.

ACKNOWLEDGMENTS

We are grateful for the helpful discussion with E. P. Houwman. The authors acknowledge support from Nanyang Technological University and Ministry of Education of Singapore under Project No. ARC 16/08. Partial support from National Research Foundation of Singapore under Project NRF-CRP5-2009-04 is also acknowledged.

*jlwang@ntu.edu.sg

[1] J. Mannhart and D. G. Schlom, Science **327**, 1607 (2010).
[2] P. Zubko, S. Gariglio, M. Gabay, P. Ghosez, and J.-M. Triscone, Annu. Rev. Cond. Mat. Phys. **2**, 141 (2011).
[3] J. Chakhalian, A. J. Millis, and J. Rondinelli, Nat. Mater. **11**, 92 (2012).
[4] H. Y. Hwang, Y. Iwasa, M. Kawasaki, B. Keimer, N. Nagaosa, and Y. Tokura, Nat. Mater. **11**, 103 (2012).
[5] R. Ramesh and N. A. Spaldin, Nat. Mater. **6**, 21 (2007).
[6] L. W. Martin, Y. H. Chu, and R. Ramesh, Mater. Sci. Eng., R **68**, 89 (2010).
[7] L. W. Martin and D. G. Schlom, Curr. Opin. Solid State Mater. Sci. **16**, 199 (2012).
[8] P. Yu, Y.-H. Chu, and R. Ramesh, Mater. Today **15**, 320 (2012).
[9] P. Yu, J. S. Lee, S. Okamoto, M. D. Rossell, M. Huijben, C. H. Yang, Q. He, J. X. Zhang, S. Y. Yang, M. J. Lee, Q. M. Ramasse, R. Erni, Y. H. Chu, D. A. Arena, C. C. Kao, L. W. Martin, and R. Ramesh, Phys. Rev. Lett. **105**, 027201 (2010).
[10] S. M. Wu, S. A. Cybart, P. Yu, M. D. Rossell, J. X. Zhang, R. Ramesh, and R. C. Dynes, Nat. Mater. **9**, 756 (2010).
[11] S. M. Wu, S. A. Cybart, D. Yi, J. M. Parker, R. Ramesh, and R. C. Dynes, Phys. Rev. Lett. **110**, 067202 (2013).
[12] M. Huijben, P. Yu, L. W. Martin, H. J. A. Molegraaf, Y. H. Chu, M. B. Holcomb, N. Balke, G. Rijnders, and R. Ramesh, Adv. Mater. **25**, 4739 (2013).
[13] L. You, C. Lu, P. Yang, G. Han, T. Wu, U. Luders, W. Prellier, K. Yao, L. Chen, and J. Wang, Adv. Mater. **22**, 4964 (2010).
[14] M. Jaafar, J. Gómez-Herrero, A. Gil, P. Ares, M. Vázquez, and A. Asenjo, Ultramicroscopy **109**, 693 (2009).
[15] E. P. Houwman, G. Maris, G. M. De Luca, N. Niermann, G. Rijnders, D. H. A. Blank, and S. Speller, Phys. Rev. B **77**, 184412 (2008).
[16] R. D. Gomez, in *Experimental Methods in the Physical Sciences*, edited by G. Marc De and Y. Zhu, Vol. 36 (Academic Press, San Diego, 2001), p. 69.
[17] Y. H. Chu, M. P. Cruz, C. H. Yang, L. W. Martin, P. L. Yang, J. X. Zhang, K. Lee, P. Yu, L. Q. Chen, and R. Ramesh, Adv. Mater. **19**, 2662 (2007).
[18] C. J. M. Daumont, S. Farokhipoor, A. Ferri, J. C. Wojdeł, J. Íñiguez, B. J. Kooi, and B. Noheda, Phys. Rev. B **81**, 144115 (2010).
[19] L. You, E. Liang, R. Guo, D. Wu, K. Yao, L. Chen, and J. L. Wang, Appl. Phys. Lett. **97**, 062910 (2010).
[20] G. Catalan and J. F. Scott, Adv. Mater. **21**, 2463 (2009).
[21] See Supplemental Material at http://link.aps.org/supplemental/10.1103/PhysRevB.88.184426 for additional figures and movies mentioned in the text.
[22] U. Hartmann, Annu. Rev. Mater. Sci. **29**, 53 (1999).
[23] H. Boschker, J. Kautz, E. P. Houwman, G. Koster, D. H. A. Blank, and G. Rijnders, J. Appl. Phys. **108**, 103906 (2010).
[24] U. Memmert, P. Leinenbach, J. Lösch, and U. Hartmann, J. Magn. Magn. Mater. **190**, 124 (1998).
[25] P. Leinenbach, J. Lösch, U. Memmert, and U. Hartmann, Appl. Phys. A **66**, 1191 (1998).
[26] K. J. Harte, J. Appl. Phys. **39**, 1503 (1968).
[27] N. J. Gökemeijer, T. Ambrose, and C. L. Chien, Phys. Rev. Lett. **79**, 4270 (1997).
[28] J. T. Heron, M. Trassin, K. Ashraf, M. Gajek, Q. He, S. Y. Yang, D. E. Nikonov, Y. H. Chu, S. Salahuddin, and R. Ramesh, Phys. Rev. Lett. **107**, 217202 (2011).
[29] M. Trassin, J. D. Clarkson, S. R. Bowden, J. Liu, J. T. Heron, R. J. Paull, E. Arenholz, D. T. Pierce, and J. Unguris, Phys. Rev. B **87**, 134426 (2013).
[30] T. H. E. Lahtinen, J. O. Tuomi, and S. van Dijken, Adv. Mater. **23**, 3187 (2011).
[31] T. H. E. Lahtinen, K. v. J. A. Franke, and S. van Dijken, Sci. Rep. **2**, 258 (2012).
[32] F. Tsui, M. C. Smoak, T. K. Nath, and C. B. Eom, Appl. Phys. Lett. **76**, 2421 (2000).
[33] H. Boschker, M. Mathews, E. P. Houwman, H. Nishikawa, A. Vailionis, G. Koster, G. Rijnders, and D. H. A. Blank, Phys. Rev. B **79**, 214425 (2009).
[34] M. Mathews, F. M. Postma, J. C. Lodder, R. Jansen, G. Rijnders, and D. H. A. Blank, Appl. Phys. Lett. **87**, 242507 (2005).
[35] Z.-H. Wang, G. Cristiani, and H. U. Habermeier, Appl. Phys. Lett. **82**, 3731 (2003).

[36]X. Ke, M. S. Rzchowski, L. J. Belenky, and C. B. Eom, Appl. Phys. Lett. **84**, 5458 (2004).
[37]M. Ziese, I. Vrejoiu, E. Pippel, P. Esquinazi, D. Hesse, C. Etz, J. Henk, A. Ernst, I. V. Maznichenko, W. Hergert, and I. Mertig, Phys. Rev. Lett. **104**, 167203 (2010).
[38]J. Nogues and I. K. Schuller, J. Magn. Magn. Mater. **192**, 203 (1999).
[39]J. A. Boschker, Ph.D. thesis, University of Twente, 2011.
[40]A. Glazer, Acta Crystallogr. Sect. B **28**, 3384 (1972).
[41]F. Kubel and H. Schmid, Acta Crystallogr. Sect. B **46**, 698 (1990).
[42]A. Vailionis, H. Boschker, W. Siemons, E. P. Houwman, D. H. A. Blank, G. Rijnders, and G. Koster, Phys. Rev. B **83**, 064101 (2011).